Journal of Catalysis 394 (2021) 387–396

Contents lists available at ScienceDirect

Journal of Catalysis

journal homepage: www.elsevier.com/locate/jcat

Creating Brønsted acidity at the SiO_2-Nb_2O_5 interface

Andrew T.Y. Wolek [a], M. Alexander Ardagh [a], Hien N. Pham [c], Selim Alayoglu [b], Abhaya K. Datye [c], Justin M. Notestein [a,*]

[a] Department of Chemical and Biological Engineering, Northwestern University, 2145 Sheridan Rd., Evanston, IL 60208, United States
[b] Center for Catalysis and Surface Science, Northwestern University, 2145 Sheridan Rd., Evanston, IL 60208, United States
[c] Department of Chemical and Biological Engineering and Center for Micro-Engineered Materials, University of New Mexico, Albuquerque, NM 87131, United States

ARTICLE INFO

Article history:
Received 7 July 2020
Revised 5 October 2020
Accepted 25 October 2020
Available online 9 November 2020

Keywords:
Overcoated materials
Hydroalkoxylation
Tetrahydropyranylation
Mixed oxides
Brønsted acids
Niobic acid

ABSTRACT

Catalytically active acid sites associated with the silica-niobia interface were probed with a series of overcoated SiO_2 on Nb_2O_5 (SiO_2/Nb_2O_5) mixed oxide materials prepared by deposition of tetraethyl orthosilicate onto niobic acid ($Nb_2O_5{\cdot}nH_2O$) or calcined niobia (Nb_2O_5). NH_3 TPD and pyridine DRIFTS studies indicated that the speciation of acid sites in the materials evolved as a function of SiO_2 loading, impacting the quantity and stability of Brønsted sites. Catalyst activity was highly dependent on SiO_2 loading in the liquid phase hydroalkoxylation of dihydropyran with n-octanol. At SiO_2 surface densities corresponding to approximately 1 Si per 2 surface Nb, the activity of these catalysts passed through a maximum approximately 20 times higher than the activity of calcined Nb_2O_5. Apparent reaction barriers measured over the most active SiO_2/Nb_2O_5 catalysts were 10 kJ/mol lower than those measured over niobic acid, suggesting that the OH features unique to the SiO_2-Nb_2O_5 interface were slightly more reactive than those on niobic acid.

1. Introduction

The catalytic properties of niobium-based oxides have received increasing interest since pioneering studies by Tanabe et al. in the 1980's reported the use of NbO_x as a promoter, SMSI support, and acid catalyst [1]. In particular, hydrated niobium oxides, also referred to as niobic acid ($Nb_2O_5{\cdot}nH_2O$), have been extensively studied due to their strong Brønsted acid character, equivalent to 70% sulfuric acid, and catalytic stability in the presence of water [2–4]. While these properties make niobic acid a promising catalyst for liquid phase reactions, the material loses acidity when heated to elevated temperatures such as might be needed for vaporized reactants or to calcine the catalyst during a regeneration step, limiting its commercial applications [1,5].

The inclusion of secondary oxide phases, such as WO_3, ZrO_2, Al_2O_3, and SiO_2, is one strategy to improve the Brønsted acidic properties of bulk niobium oxides [6–8]. Among these, niobia-silica oxides in particular have been successfully synthesized by a wide variety of techniques. Mixed oxides have been synthesized by routes including sol–gel, solution thermolysis, and co-precipitation, and they have exhibited increased thermal stability and decreased deactivation in the presence of water [9–12]. Brønsted acidity has also been identified in supported NbO_x/SiO_2 (e.g. niobia on silica) and NbO_x/Al_2O_3 materials, with strong Brønsted sites forming at sub-monolayer coverages of NbO_x [13,14]. A complicating factor in understanding NbO_x/SiO_2 materials is that NbO_x domains grow and change structure (e.g. from isolated sites to monolayers) with increasing surface density, while the niobia-silica interface also changes structure. This can make it challenging to separate the importance of these two factors.

The acidity of the reverse materials, consisting of SiO_2 deposited on niobium oxides (SiO_2/Nb_2O_5), is not currently known. The catalytic dehydration and isomerization activity of comparable SiO_2/ZrO_2 and SiO_2/TiO_2 materials have been studied as a function of Si surface density [15], and we and others have examined Brønsted acidity at the SiO_2/Al_2O_3 interface [16–18]. Beyond improved performance metrics, these materials have yielded additional understanding of the new active sites that arise at the mixed oxide interfaces because the deposited SiO_2 is, on its own, catalytically inert, and because the bulk structure of the underlying metal oxide does not depend on loading, unlike their supported oxide counterparts. In this work, we prepare a series of overcoated silica on niobia (SiO_2/Nb_2O_5) materials, tracking the evolution of surface species as a function of surface SiO_2 density and measuring their activity in the hydroalkoxylation of dihydropyran with n-octanol, which is used here as a probe reaction that requires Brønsted acidity.

* Corresponding author.

https://doi.org/10.1016/j.jcat.2020.10.027
0021-9517/

2. Experimental methods

2.1. Synthesis

SiO_2 was grafted onto niobic acid ($Nb_2O_5{\cdot}nH_2O$, HY-340, CBMM) by adapting a base-catalyzed methodology previously used by some of us to deposit thin films of SiO_2 onto Al_2O_3 and TiO_2 supports [16,19]. This synthesis method was suitable for multi-gram syntheses without specialized equipment, facilitating subsequent characterization efforts. In summary, 2 g of niobic acid was taken as received and added to a solution of 6.7:1 parts ethanol (200 proof; Fisher) and NH_4OH (28% in H_2O, Fisher). The niobic acid was then suspended in the solution by sonicating at room temperature for 30 min. Following this 70, 140, or 260 μL of tetraethyl orthosilicate (TEOS, ≥99%, Aldrich), corresponding to 0.6, 1.2, or 2.4 molecules / nm^2 was injected into the mixture and allowed to react for 1 h while shaking on a gyratory plate. These conditions correspond to samples 0.6-SiO_2/Nb_2O_5, 1.2-SiO_2/Nb_2O_5, 2.4-SiO_2/Nb_2O_5, which are named according to the surface loading of deposited metal normalized relative to the surface area of niobic acid in units of atoms / nm^2. The SiO_2 overcoat in these samples is sub-monolayer as the Nb surface density on niobic acid is ~5 Nb atoms / nm^2 [20].

For higher SiO_2 loadings, the above procedure was carried out using 280 μL TEOS, corresponding to 2.5 molecules / nm^2. After 1 hr shaking, the samples were re-sonicated for 30 min to re-suspend, then an additional 120 μL TEOS was injected and allowed to react for 1 h while shaking, to give sample 3.6-SiO_2/Nb_2O_5. The cycles of re-sonication and addition of 120 μL TEOS were repeated 3 and 14 additional times for samples 8.6-SiO_2/Nb_2O_5 and 28.5-SiO_2/Nb_2O_5, respectively. A smaller amount of TEOS was injected during these higher cycles to compensate for the lower OH density expected on the SiO_2 overcoat compared to the underlying niobic acid. Note that we were unable to precisely determine the OH density of the niobic acid by thermogravimetric analysis due to its high H_2O content and thermal sensitivity.

After completing the deposition process, samples were washed twice with 200 mL ethanol and once with 200 mL hexanes (Fisher) before being collected by vacuum filtration. Samples were allowed to dry with vacuum applied overnight before being collected. Calcined niobic acid, referred hereafter as calcined Nb_2O_5, was prepared by calcining as-obtained $Nb_2O_5{\cdot}nH_2O$ at 550 °C in static air for 3 h with a 3 °C / min ramp rate. A set of SiO_2 on calcined Nb_2O_5 controls were prepared by following the SiO_2 deposition procedure outlined above, but starting with calcined Nb_2O_5. These controls are named using the previously described nomenclature with an additional Nb_2O_5–c label. All materials were activated by calcining at 550 °C in static air for 3 h. A 3 °C / min ramp rate was used, as we have previously identified this parameter to influence SiO_2 overcoat properties [16]. Samples were stored in a desiccator and were reactivated by calcining at 300 °C overnight if not used within 30 days.

2.2. Characterization

SiO_2 loadings for the series of catalysts were determined by inductively coupled plasma optical emission spectroscopy (ICP-OES) conducted on a Thermo iCAP 7600 in the Quantitative Bioelement Imaging Center (QBIC) at Northwestern University. Samples were digested in 48 wt% HF (Fisher), shaken at 200 rpm for 24 h, then diluted with 1 wt% HNO_3 (Fisher). [CAUTION: Store and handle HF with extreme care]. Optical emission spectra were calibrated against a standards curve prepared by dilution of commercial Si standard (Sigma-Aldrich). Reported values are averages of triplicates conducted for each sample.

Transmission electron microscopy (TEM) images were acquired on a JEOL-2010F with an accelerating voltage of 200 kV. Samples were prepared by dispersing solids in ethanol then mounted on a holey carbon TEM grid. Images were recorded in both bright field (BF) and high angle annular dark field (HAADF) modes.

BET surface area and BJH pore volumes were calculated from N_2 physisorption isotherms collected at 77 K on a Micromeritics 3FLEX instrument in the REACT core facility at Northwestern University. All materials were degassed prior to treatment by holding at 250 °C under dynamic vacuum (<5 mm Hg) overnight. BET surface areas were estimated over a relative pressure range of 0.05 to the maximum of the Rouquerol plot [21], typically ~0.50 P/P_0. BJH pore volumes were calculated from the desorption branch of the isotherms. Pore size distributions were calculated using Non-Local Density Functional Theory (NLDFT) with a N_2 cylindrical pore model for oxides and a regularization value of 0.2000 [22,23].

X-ray diffraction scattering patterns were acquired on a Rigaku Ultima PXRD in the Jerome B. Cohen X-Ray Diffraction Facility at Northwestern University. Samples were scanned with a Cu K-α source from 5° to 90° 2-θ in glass sample pans and the diffraction patterns were identified using MDI JADE 9 fitting software (Materials Data Inc., USA).

Catalyst acid properties were studied with NH_3 temperature programmed desorption (TPD), propylamine temperature programmed reaction (TPRx), and diffuse reflectance infrared Fourier transform spectroscopy (DRIFTS) using pyridine and NH_3 as probe molecules in the REACT core facility at Northwestern University. Typical NH_3 TPD experiments involved pretreating the catalyst at 300 °C in 30 sccm of 10% O_2 / 90% He for 30 min before the sample was saturated with 10% NH_3 / 90% He at 100 °C. Following this, UHP He was flown at 30 sccm to purge physisorbed NH_3 from the system, and the samples were heated to 600 °C at 10 °C / min under the same flow NH_3 desorption (m/z = 17) was monitored by inline MS.

Propylamine TPRx (Hoffmann elimination reaction) was used to selectively quantify Brønsted acid sites. In a typical experiment, samples were pretreated at 300 °C in 30 sccm of UHP He for 30 min before cooling to 100 °C for propylamine chemisorption. Samples were saturated with propylamine (>99%, Alfa) by flowing 10 sccm UHP He through a bubbler held at 3 °C, providing ~17% propylamine flow. Physisorbed proyplamine was purged by flowing 30 sccm UHP He before samples were heated to 550 °C at 10 °C / min to catalytically decompose the propylamine to form propylene and NH_3. Desorption of propylamine (m/z = 30) and reaction products were monitored by inline MS, with NH_3 (m/z = 17) and propylene (m/z = 41) desorption peak areas found to be equivalent within error. Propylamine decomposition occurs at ~400 °C regardless of Brønsted strength, producing a sharp propylene elution peak and limiting the possibility that propylamine desorbs and reacts on a secondary Brønsted site [24]. We have used the propylene signal for quantification since NH_3 desorption was significantly broadened by the chromatographic effect.

Pyridine DRIFTS experiments were performed on a Thermo Nicolet 6700 FTIR spectrometer with a praying mantis diffuse reflectance sample holder. Sample spectra as shown are the average of 64 scans each with a resolution of 0.5 cm^{-1}. Samples were diluted ~10 wt% in KBr and pretreated at 300 °C under 40 sccm 10% O_2 / 90% Ar for 30 min. Following cooling to 150 °C, background spectra were obtained and 100 uL of pyridine (≥99.0%, Sigma) was injected into a heated sample loop and introduced to the system with 40 sccm of UHP Ar carrier gas. After the pyridine had saturated the samples, vacuum was pulled for 1 h and the final spectra were acquired. Pyridine desorption was studied by heating samples to 200 °C or 250 °C for 30 min under vacuum before cooling to 150 °C for spectra collection. The acquired diffuse reflectance spectra were processed by applying the Kubelka-Munk transformation with OMNIC FTIR software (Thermo Scientific).

2.3. Catalytic reactions

Liquid phase hydroalkoxylation of dihydropyran with n-octanol was studied with batch reactions run in excess 3,4-dihydro-2H-pyran (DHP, molar ratio DHP:n-octanol = 2). Prior to reaction, previously calcined catalysts were re-activated by drying at 300 °C overnight in static air. In a typical reaction, 15 mg catalyst was weighed hot into 20 mL glass vials to minimize readsorption of moisture. 7 mL of preheated reaction solution (0.6 mmol 1-octanol (≥99%, Sigma), 1.2 mmol DHP (97%; Aldrich), 0.6 mmol mesitylene internal standard (98%, Sigma) in heptane (99%, Sigma)) was then dosed and allowed to react on a heated shaker plate at 500 rpm and 70 °C. Samples (50 μL) were taken periodically via syringe equipped with a Whatman 0.7 um glass microfiber filter and analyzed on a Shimadzu GC 2010-plus equipped with a MS detector and a 30 m Zebron ZB-624 capillary column. Triplicate reactions were run for each catalyst and initial reaction rates were calculated by quantifying the production of the tetrahydropyranyl ether over the first 15 min of the reaction. Mass balances were >95% based on octanol and octyl-containing products.

3. Results and discussion

3.1. SiO_2 overcoating of $Nb_2O_5{\cdot}nH_2O$

Previously reported techniques were adapted to study the SiO_2 / bulk Nb_2O_5 interface which has not been investigated as thoroughly as its inverse, supported NbO_x on bulk SiO_2 [16,19]. A summary of physical characterization for the series of prepared SiO_2/Nb_2O_5 materials and associated controls is shown in Table 1. Sample information for additional SiO_2/Nb_2O_5 materials used primarily in catalyst testing is located in Supporting Information Table S1.

Thermal treatment of niobic acid at temperatures above 500 °C has been previously shown to result in extensive structural changes, crystallization, and a near complete loss of Brønsted acidity [2,5,25]. In contrast, HAADF-STEM images of calcined 3.6-SiO_2/Nb_2O_5 (Fig. 1b) show the material primarily retains the original niobic acid morphology (Fig. 1a). While we did observe some localized crystallization in the sample, (Supporting Information Fig. S2), the majority of the sample remained amorphous, as shown by absence of a regular lattice in Fig. 1d. When comparing HRTEM images of niobic acid (Fig. 1c) and 3.6-SiO_2/Nb_2O_5 (Fig. 1d), we see the SiO_2 overcoat is close to 1 nm in thickness. SiO_2 deposition did not yield a perfect monolayer, which would be largely invisible at this scale, but neither did it yield large regions of bulk SiO_2. Deposition of much larger amounts of SiO_2 (shown in Supporting Information Fig. S2) results in a less homogeneous catalyst, where all niobic acid is encapsulated in SiO_2, but some particles have substantially more SiO_2 deposition than others. The structural heterogeneity of the high-loaded samples is not a cause for significant concern, as these materials are poorly active for catalysis.

Sample N_2 isotherms and NLDFT pore size distributions are located in Supporting Information Figs. S3 and S4, respectively. In agreement with literature, calcining niobic acid at 550 °C results in a ~85 m^2 / g decrease in surface area [25]. The calcined, overcoated materials show a monotonic drop in the BJH pore volume with increasing SiO_2 loading, but for most SiO_2 loadings, they retain more surface area than does the uncoated catalyst. The pore size distributions (Supporting Information Fig. S4) show that SiO_2 deposition partially stabilizes the 2–4 nm pores in the original niobic acid, which otherwise disappear when niobic acid is calcined.

X-ray diffraction patterns, shown in Fig. 2, confirm that the calcination conditions are enough to crystallize uncoated niobic acid into Nb_2O_5. With major peaks at 22.7°, 28.6°, and 36.7° 2-θ, the crystal phases present in the calcined Nb_2O_5 sample were identified as 80 wt% TT-Nb_2O_5 (hexagonal, PDF# 00-028-0317) and 20 wt% T-Nb_2O_5 (orthorhombic, PDF# 01-071-0336). We note the mixed phase composition of calcined Nb_2O_5 is consistent with the Nb_2O_5 phase progression put forth by other studies [25,26].

As expected, XRD of calcined SiO_2/Nb_2O_5 samples does not detect any crystalline SiO_2 phases, since the calcination temperatures used are significantly lower than those needed for the amorphous silica to cristobalite phase transformation [27]. However, crystallization of the Nb_2O_5 core to TT-Nb_2O_5 and T-Nb_2O_5 phases is observed in low SiO_2 content samples 0.6-SiO_2/Nb_2O_5 and 1.2-SiO_2/Nb_2O_5. At higher SiO_2 loadings, the major crystalline Nb_2O_5 reflections at 22.7° and 28.6° are still present but secondary to the amorphous character of the samples, indicating incomplete crystallization of the core oxide, which is consistent with the TEM images of 3.6-SiO_2/Nb_2O_5 in Fig. 1.

Other reports have indicated that thin films deposited by atomic layer deposition have similar impacts on phase transitions in Fe_2O_3 and Nb_2O_5 systems [28–30]. We hypothesize that limited Nb mobility at the Nb-O-Si interface is slowing Nb_2O_5 crystallization [31], rather than increasing the phase transition temperature. To investigate further, we calcined samples 2.4-SiO_2/Nb_2O_5 and 28.5 SiO_2/Nb_2O_5 for an additional 24 h, and indeed, XRD patterns of both samples obtained after the additional 24 h hold show complete crystallization to T-Nb_2O_5 and TT-Nb_2O_5 (Supporting Information Fig. S5). In summary, the SiO_2 deposition process creates an overcoat of sub- to multi-layer amorphous SiO_2. The presence of this overcoat reduces the extent of the structural changes that niobic acid undergoes at temperatures above 500 °C and slows the core oxide's crystallization to T- and TT-Nb_2O_5.

3.2. NH_3 desorption and propylamine decomposition studies

After identifying the physical effects associated with SiO_2 deposition, we set out to quantify the surface acidity of the materials. We first probed the strength of Brønsted sites via chemisorption of Hammett indicators (Supporting Information Fig. S7). This method has been extensively used to characterize the acidity of niobic acid and Nb_2O_5 based materials [10,32–34]. These

Table 1
Physical properties of SiO_2/Nb_2O_5 materials.

material	SiO_2 content (wt%)[a]	calculated Si surface density (Si atom/ nm^2)	BET surface area (m^2 / g)[b]	BJH pore volume (cc / g)	included analysis
niobic acid	n.d.	–	151	0.16	*c,d,e,f,h*
calcined Nb_2O_5	n.d.	–	67	0.16	*c,d,e,f,h*
0.6-SiO_2/Nb_2O_5	0.9	0.6	78	0.16	*c,h*
1.2-SiO_2/Nb_2O_5	1.9	1.2	81	0.14	*c,h*
2.4-SiO_2/Nb_2O_5	3.6	2.4	78	0.13	*d,g*
3.6-SiO_2/Nb_2O_5	5.4	3.6	85	0.13	*c,d,e,f,h*
8.6-SiO_2/Nb_2O_5	13.0	8.6	55	0.07	*e,f,h*
28.5-SiO_2/Nb_2O_5	43.0	28.5	27	0.04	*c,d,e,f,h*

a Accurate to ±10% relative; *b* Accurate to ±5 m^2/g; *c* TEM; *d* XRD; *e* NH_3 TPD and propylamine TPRx; *f* pyridine and NH_3 DRIFTS; *g* Hammett indicators; *h* octanol

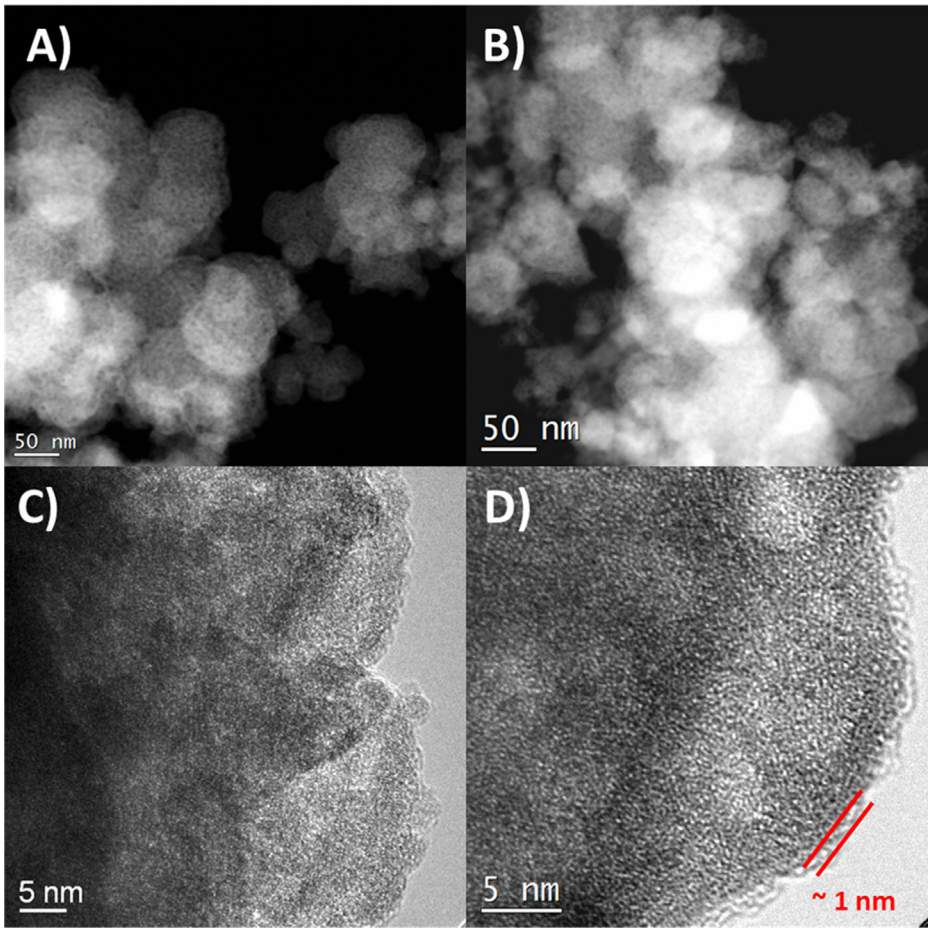

Fig. 1. Representative HAADF-STEM images of a) niobic acid, b) calcined 3.6-SiO_2/Nb_2O_5, and HRTEM images of c) niobic acid d) calcined 3.6-SiO_2/Nb_2O_5. Visible in d), the deposited SiO_2 is ~1 nm in thickness. Additional TEM images are located in Supporting Information Fig. S2.

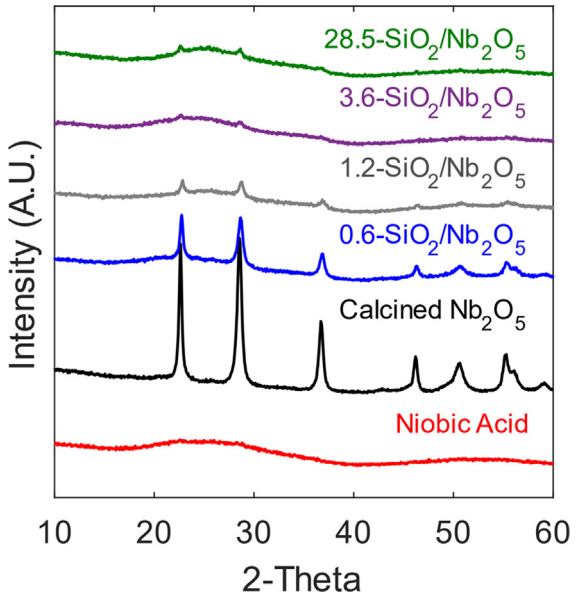

Fig. 2. X-Ray diffraction patterns of SiO_2/Nb_2O_5 materials.

experiments suggest that SiO_2/Nb_2O_5, niobic acid, and calcined Nb_2O_5 contain Brønsted sites of similar strength between $-2.4 < pKa\ (aq.) < -6.2$. However, the limited resolution of these experiments led us to next quantify surface acidity via gas phase desorption of basic probe molecules. NH_3 was chosen as an appropriate starting probe due to its small kinetic diameter (0.26 nm) that allows it to probe most structurally hindered sites [16,35–37]. Temperature programmed desorption of NH_3 was conducted for select SiO_2/Nb_2O_5 samples to study the evolution of acid sites as SiO_2 loading was increased. Total acidity counts are listed in Table 2 on a mass and surface area basis.

Table 2
NH_3 and propylamine temperature programmed desorption.

material	NH_3 uptake		Propylamine reacted	
	μmol/ g_{Nb2O5}	molec./ $nm^2 \times 10^2$	μmol/ g_{Nb2O5}	molec./ $nm^2 \times 10^2$
niobic acid	83	33	25	10.
calcined Nb_2O_5	25	22	2	1.8
0.6-SiO_2/Nb_2O_5	50	39	9	6.9
3.6-SiO_2/Nb_2O_5	41	31	3	2.1
8.6-SiO_2/Nb_2O_5	22	28	2	2.2
28.5-SiO_2/Nb_2O_5	3	10	1	2.2

Although niobic acid has been reported to be a promising acid catalyst at low to moderate temperatures, heating it to elevated temperatures is known to eliminate both Lewis and Brønsted acid sites [1,5]. The loss of sites from moderate thermal treatment (<300 °C) can be reversed by exposure to water vapor but becomes irreversible once niobic acid crystalizes to Nb_2O_5 [32]. We observe

a decrease of ~70% (mass basis) or ~30% (surface area basis) in total NH_3 uptake after calcining niobic acid to form crystalline T- and TT-Nb_2O_5, consistent with previous reports. Interestingly, the SiO_2/Nb_2O_5 materials adsorb more NH_3 than calcined Nb_2O_5 at all but the highest SiO_2 loadings, and at moderate SiO_2 loadings, the SiO_2/Nb_2O_5 materials adsorb comparable or even slightly higher amounts of NH_3 per unit surface area than niobic acid. As SiO_2 loadings are increased, the NH_3 absorption generally decreases, leading to minimal detectable acidity over 28.5-SiO_2/Nb_2O_5, as expected for a purely siliceous surface.

The shape of NH_3 desorption profiles provides some insight into the speciation of acid sites, since NH_3 desorbs from stronger acid sites at higher temperatures. In Fig. 3a, the raw TPD data for each sample are fit to a series of three Gaussians centered at approximately 200 °C, 260 °C, and 370 °C. We tentatively assign these features to weakly acidic surface hydroxyls, medium Lewis sites, and a combination of strong Lewis + Brønsted sites, respectively [38–41]. Fig. 3b shows the relative contributions from each population as a function of the Si surface density. Looking at the relative contributions, it is apparent that the significant decrease in total NH_3 uptake in the calcined Nb_2O_5 sample is mainly due to the loss of medium and strong acid sites. Interestingly, we observe an increased amount of both medium and strong acid sites relative to calcined Nb_2O_5 in the series of SiO_2/Nb_2O_5 materials. The quantity of these acid sites is maximized at sub-monolayer SiO_2 loadings, with the number of strong acid sites in the 0.6-SiO_2/Nb_2O_5 sample being roughly double that of calcined Nb_2O_5 (mass basis). As the SiO_2 loading is further increased we observe a decrease in medium and strong acid sites until only contributions from weak acid sites are detected over 28.5-SiO_2/Nb_2O_5, again as we expect for a siliceous surface. We note that we were only able to obtain a good fit for niobic acid when fitting the strong acid feature ~60 °C higher (430 °C) than we did in the SiO_2/Nb_2O_5 samples, suggesting unique populations of acid sites on the two types of surfaces.

Propylamine decomposition was used as an additional basic probe to quantify the number of Brønsted acid sites [24,35,42–44]. Propylamine adsorbs on both Lewis and Brønsted sites, but it only decomposes to NH_3 and propylene on Brønsted acid sites and at ~400 °C [24], meaning that the method only counts strong sites able to retain propylamine at these elevated temperatures [45]. In qualitative agreement with previous reports and our with NH_3 desorption results, there is a ~80% (surface area basis) decrease in the number of Brønsted acid sites quantified by propylamine decomposition when niobic acid is calcined [1,5]. Relative to calcined Nb_2O_5 we observe the number of Brønsted sites in the SiO_2/Nb_2O_5 materials increase at low SiO_2 loadings before converging to comparable values. At the local maximum centered at 0.6 Si / nm^2, the Brønsted site density is 3.8 times (surface area basis) greater than that of calcined Nb_2O_5.

The thermal stability of these materials was tested by repeating the propylamine decomposition experiments for a total of three cycles. Each cycle was treated as an individual experiment with its own pretreatment at 300 °C, propylamine saturation, and TPRx ramp. Fig. 4 shows a progressive loss in acidity for both niobic acid and 0.6-SiO_2/Nb_2O_5, indicating both materials are metastable. Raw TPRx data and tabulated data for additional samples are located in Supporting Information Figs. S8 and S9, respectively. Niobic acid saw the largest decrease after the first TPRx cycle, with a loss of 8.2×10^{-2} molec. / nm^2, corresponding to ~82% the original Brønsted sites. The loss of sites is due to the evolution of moisture from the sample, since we observed a moderate water signal during the first desorption cycle. The SiO_2/Nb_2O_5 samples also showed progressively fewer Brønsted sites with sequential cycles, although none exhibited as severe a decrease as niobic acid. Critically, the 0.6-SiO_2/Nb_2O_5 sample was more thermally stable than niobic acid, retaining a larger absolute number of Brønsted sites in the second and third TPRx cycles.

Together, the NH_3 TPD and propylamine TPRx experiments show that the number and distribution of acid sites in the SiO_2/

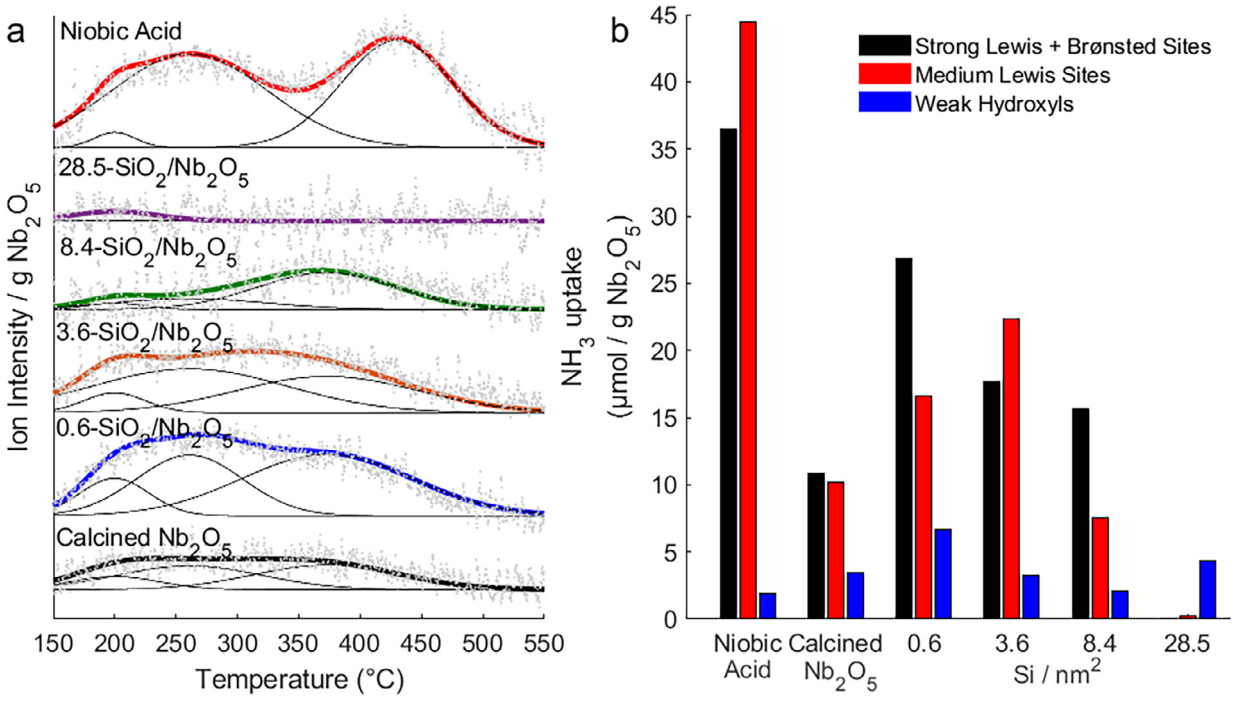

Fig. 3. (Left) Raw NH_3 TPD profiles for select SiO_2/Nb_2O_5 materials and controls and data fit overlays. Profiles were fit to m/z = 17 NH_3 fragment signal. (Right) Relative contributions of fit components as function of SiO_2 loading (mass basis). The relative fit contributions are tabulated on both mass and surface area bases in Supporting Information Table S6.

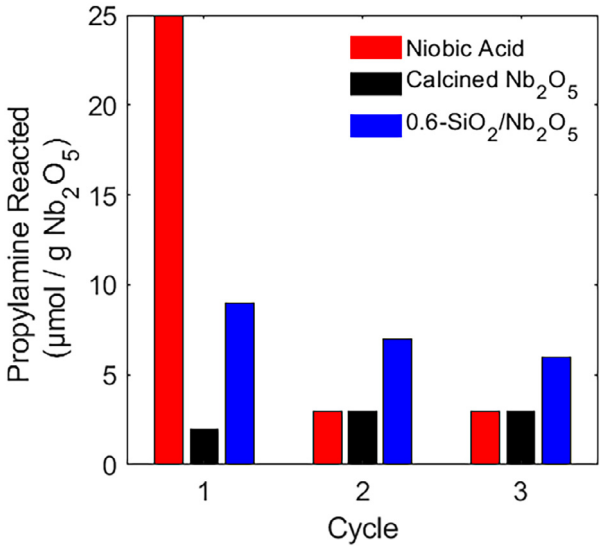

Fig. 4. Cyclic propylamine decomposition for SiO_2/Nb_2O_5 materials.

Nb_2O_5 materials is highly dependent on the SiO_2 loading, with low loadings increasing the number of medium and strong acid sites relative to calcined Nb_2O_5 and higher loadings leading to a decrease in the number of these acid sites. Additionally, our cyclic propylamine TPRx experiments suggest that Brønsted acid sites in the SiO_2 overcoated materials have increased thermal stability compared to those in niobic acid.

3.3. DRIFTS studies of surface acid sites

IR experiments with NH_3 and pyridine probes were used to spectroscopically differentiate the types of acid sites present in samples. Both probes gave qualitatively similar results. The NH_3 DRIFTS spectra are discussed in Supporting Information Fig. S11. Pyridine has strong gas-phase basicity and distinct Lewis and Brønsted acid binding modes [46], and is discussed in depth here. IR spectra were collected in diffuse reflectance mode since significant absorbance of IR light by Nb_2O_5 precluded operation in transmission mode. Fig. 5 shows the hydroxyl and ring stretching regions of the pyridine difference spectra for niobic acid and select SiO_2/Nb_2O_5 materials. The full pyridine DRIFTS spectra are located in Supporting Information Fig. S10.

In the OH region of the niobic acid spectra, we observe a negative feature at 3705 cm^{-1} assigned to the loss of isolated Nb-OH species following pyridine adsorption. This negative feature is no longer present in the difference spectrum after the sample is calcined to Nb_2O_5 at 550 °C [5,47]. The loss of this feature in the calcined Nb_2O_5 spectra is again consistent with the evolution of water from surface hydroxyls during thermal treatment. This feature is also largely absent in the SiO_2/Nb_2O_5 materials and is instead replaced by a negative feature at 3745 cm^{-1}, whose absolute intensity is maximized at a loading of 3.6 Si / nm^2. The shift from 3705 to 3745 cm^{-1} indicates that the surface OH species have been modified by the SiO_2 deposition. We assign the feature at 3745 cm^{-1} to pyridine adsorbing on Si-OH perturbed by proximity to the niobia surface [16,48]. We separately note that materials with high SiO_2 loadings likely have high absolute numbers of Si-OH groups, but that these Si-OH groups resemble those of bulk amorphous SiO_2, which do not appreciably adsorb pyridine and thus do not appear in the difference spectrum.

In the ring-stretching region of the spectra, we observe peaks at 1445 cm^{-1} and 1606 cm^{-1} assigned to pyridine bound to Lewis sites [5,49]. Peaks at 1540 cm^{-1} and 1639 cm^{-1} are indicative of protonated pyridinium ions on Brønsted sites. The band at 1488 cm^{-1} has been assigned to a combination of Brønsted and Lewis binding modes [49]. As SiO_2 is deposited, the Brønsted peak at 1540 cm^{-1} grows in size, reaching a maximum at 3.6 Si / nm^2 before decreasing in intensity at higher loadings. In contrast, SiO_2 deposition decreases the Lewis binding features at 1445 cm^{-1}

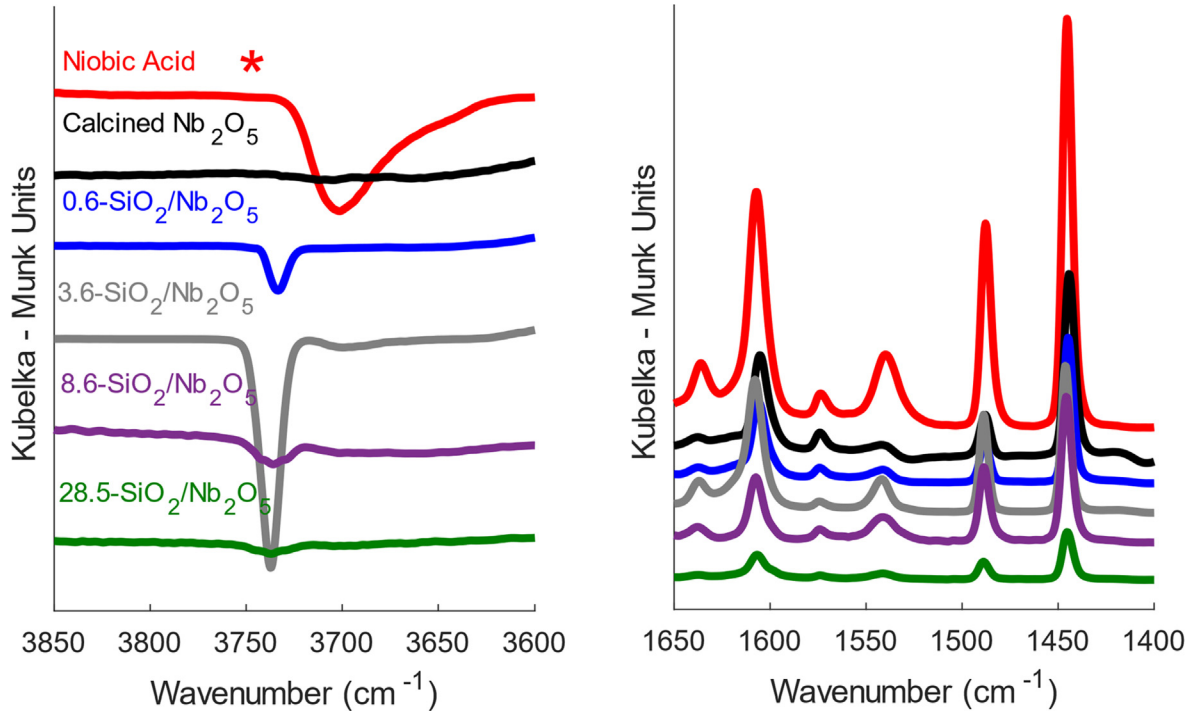

Fig. 5. Pyridine DRIFTS difference spectra for SiO_2/Nb_2O_5 materials at 150 °C. Hydroxyl bending region (left) and pyridine stretching and ring vibration region (right). * indicates half scale.

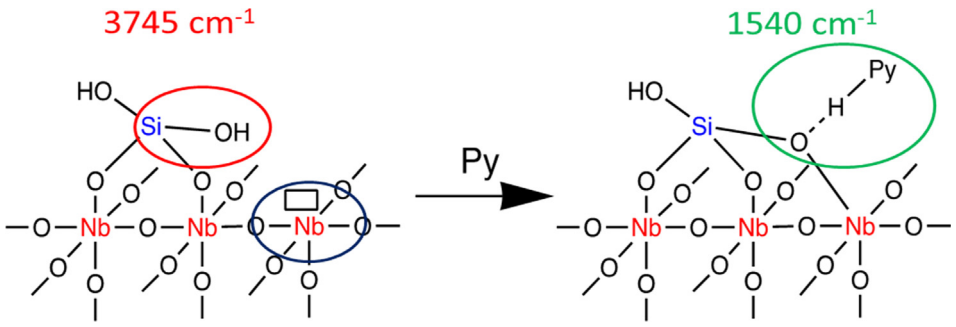

Scheme 1. Proposed pseudo-bridging silanol structure. The acid site is originally in a "open" configuration with distinct Si-OH and Nb Lewis sites that "closes" upon exposure to pyridine.

and 1606 cm^{-1} relative to niobic acid and calcined Nb_2O_5, suggesting they are either consumed or blocked by the deposition process. Finally, pyridine begins to desorb from Brønsted and Lewis sites on these materials at temperatures as low as 250 °C (Supporting Information Fig. S12), indicating that pyridine is adsorbed on a range of acid site strengths.

In aggregate, NH_3 TPD, propylamine TPRx, and pyridine DRIFTS spectra suggest that new acid sites are formed at the SiO_2-Nb_2O_5 interface as SiO_2 is deposited. In niobic acid, Lewis sites are attributed to undercoordinated NbO_x species while Brønsted sites are attributed to Nb-OH groups [32]. In SiO_2/Nb_2O_5, we attribute Lewis character to the fraction of the same undercoordinated NbO_x species that remain uncovered by SiO_2. In contrast, the shift of the OH stretch from 3705 cm^{-1} to 3745 cm^{-1} indicates the formation of new Brønsted sites in SiO_2/Nb_2O_5.

In amorphous silica alumina materials, recent DFT calculations have provided evidence that Brønsted acidity originates from pseudo-bridging silanols formed from neighboring Si-OH and Al Lewis sites [50,51]. These structures exist in an "opened" state with distinct Si-OH and Al Lewis sites that "close" to form a Si-O(H)-Al bridge when exposed to a base. We hypothesize that analogous structures are the source of Brønsted acidity in SiO_2/Nb_2O_5. Here, Si-OH species from deposited SiO_2 domains may interact with neighboring NbO_x Lewis sites to "close" and form Brønsted acidic Si-O(H)-Nb bridges (shown in Scheme 1) [52]. We note that the negative 3745 cm^{-1} Si-OH feature is maximized at the same SiO_2 loadings as the positive 1540 cm^{-1} Brønsted feature, suggesting that these pseudo-bridging sites remain "open" until exposed to pyridine. Finally, we comment that a definitive assignment of the acid site structure in these materials remains challenging given the continuing difficulty in characterizing amorphous mixed oxides [53,54].

These pseudo-bridging structures would be predicted to be most abundant at sub-monolayer SiO_2 loadings where the SiO_2 – Nb_2O_5 interface is significant and where undercoordinated NbOx still persist. As discussed in the previous section, the number of medium and strong acid sites as determined by NH_3 TPD was maximized at moderate, sub-monolayer SiO_2 loadings. Likewise, pyridine DRIFTS indicates that the SiO_2/Nb_2O_5 materials retain Lewis sites after overcoating and annealing at 550 °C while the Brønsted sites corresponding to the peak at 1540 cm^{-1} are maximized at a SiO_2 loading of 3.6 Si / nm^2 due to the interaction of a Si-OH with an adjacent, uncovered NbOx Lewis site. Finally, propylamine TPRx shows a continuous decrease in the strongest Brønsted sites as SiO_2 loading increases, suggesting that these sites may not be associated with pseudo-bridging structures at the SiO_2/Nb_2O_5 interface.

3.4. Hydroalkoxylation of dihydropyran to probe Brønsted acidity

Hydroalkoxylation, or the addition of alcohols across alkenes and alkynes, is a synthetic route that has found wide application in fine chemical and pharmaceutical synthesis [55,56]. Recent work has identified several Brønsted acid catalysts capable of obtaining high yields for both intermolecular addition and intramolecular cyclization routes [57–59]. Molecular complexes of Ru, Pt, La, and Ce have also been proven to be active for the reaction. They are hypothesized to work by either directly activating the alkene or promoting protonolysis of the reaction media [60–63].

The hydroalkoxylation of alcohols with 3,4-dihydro-2H-pyran, also known as tetrahydropyranylation (Scheme 2), is used in multistep syntheses to protect vulnerable alcohol functional groups. The reaction has been extensively employed since its discovery in the late 1960s and is commonly catalyzed by solid acids, including silica-alumina, protic ion-exchange resins, and zeolites, among other materials [55,56,64]. The reaction is easily carried out in parallel batch reactions, which for this work makes it very useful for screening catalyst materials with acid character. Furthermore, the reaction has been shown elsewhere to be sensitive to acid strength [65,66]. The reaction is first order with respect to acid concentration over relevant ranges (Supporting Information Fig. S13).

We do not observe any conversion over Lewis acidic oxides such as Al_2O_3 and TiO_2, suggesting that Brønsted acidity is a necessary – but perhaps not sufficient – requirement for the reaction under the tested conditions. Cooperativity between Brønsted and Lewis sites may also possible, since their combination has been shown to enhance reactivity in this reaction elsewhere [55,59,67]. We have plotted the initial reaction rate vs Si surface density in Fig. 6 to highlight activity trends across the series of SiO_2/Nb_2O_5 catalysts. A tabulated summary of catalytic activities on surface area and mass bases is located in Supporting Information Table S14. An alternate form of Fig. 6 plotted on a mass basis is found in Supporting Information Fig. S15.

Niobic acid, calcined Nb_2O_5, and SiO_2 were tested as moderate Brønsted acid catalysts and controls. Niobic acid showed moderate activity, reaching 45% conversion after 1 h, with an initial rate of 0.20 mmol / m^2 – h. Initial rates measured over calcined Nb_2O_5 were an order of magnitude lower (0.02 mmol / m^2 - h) as we expected based on the loss of 82% of its Brønsted sites (surface area basis) during thermal treatment. Negligible activity was measured over SiO_2. Since it appears neither the crystalline Nb_2O_5 surface nor the SiO_2 surface are highly active for this reaction, we attribute any

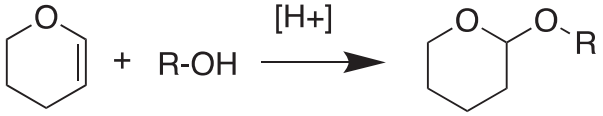

Scheme 2. Alcohol Tetrahydropyranylation.

increases in activity in the SiO_2/Nb_2O_5 samples to the newly formed silica-niobia interface.

Deposition of SiO_2 onto niobic acid resulted in a rapid increase in activity from 0.02 mmol / m^2 - h for calcined Nb_2O_5 to a maximum 0.51 mmol / m^2 – h in 3.6-SiO_2/Nb_2O_5. A similar trend is observed in the mass-normalized rates, shown in Supporting Information Fig. S15. Notably, this value is 25.5 times greater than the 0.02 mmol / m^2 - h observed over calcined Nb_2O_5. It is also ~150% greater than the 0.20 mmol / m^2 – h measured over the parent niobic acid, even though that sample had a greater quantity of total acid sites as measured by NH_3 TPD and strong Brønsted sites as measured by propylamine TPRx. We measured similarly high reaction rates over a series of SiO_2/Nb_2O_5-c controls (Supporting Information Table S14) which were synthesized by SiO_2 deposition on pre-calcined Nb_2O_5. The significant enhancement in activity for sub-monolayer loadings of SiO_2, independent of the phase of Nb_2O_5 that SiO_2 is deposited on, strongly suggests new active sites are being formed at the silica-niobia interface. Then, as SiO_2 loadings approach and exceed ~5 Si / nm^2, the activity steadily decreases, consistent with the formation of an inactive silica shell at high SiO_2 loadings. This further suggests that active sites are found at the SiO_2-Nb_2O_5 interface and rules out the formation of an active overlayer formed by diffusion of Nb into the SiO_2, or vice versa, during thermal treatments.

We determined activation energies over niobic acid and 3.6-SiO_2/Nb_2O_5 by fitting initial rates collected at 50–70 °C to an Arrhenius model (Supporting Information Fig. S16). The apparent energy barrier is slightly lower over 3.6-SiO_2/Nb_2O_5 than over niobic acid (68 kJ/mol vs. 78 kJ/mol ±5 kJ/mol), indicating that although there may be fewer acid sites in the SiO_2/Nb_2O_5 materials as measured by NH_3 TPD and propylamine TPRx, those present are more active for the tetrahydropyranylation reaction.

Finally, we calculated catalytic turnover frequencies (TOFs) based on a number of different approaches to defining an active site (Fig. S17). First, TOFs based on propylamine TPRx vary significantly from material to material, arguing against the relevance of this metric for determining catalytic active sites. The medium

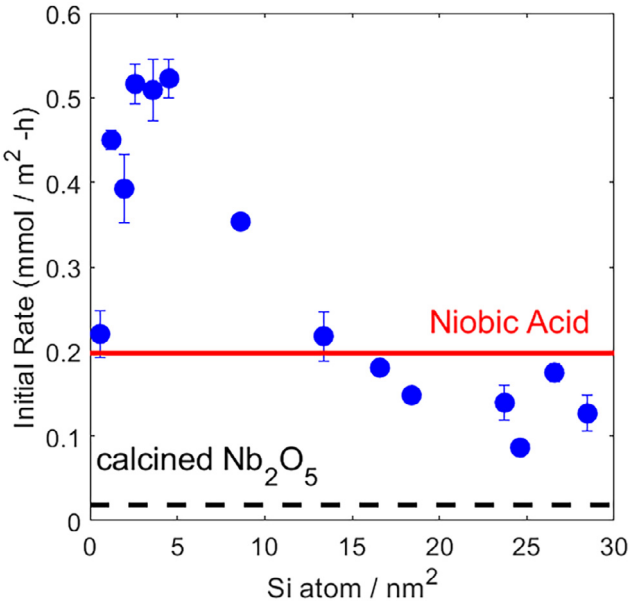

Fig. 6. Tetrahydropyranylation rates for SiO_2/Nb_2O_5 materials. Conditions: 70 °C, 500 rpm, ~15 mg catalyst in 7 mL of preheated reaction solution (0.6 mmol 1-octanol, 1.2 mmol DHP). Red line indicates activity of as-obtained niobic acid and dashed black line indicates activity of calcined Nb_2O_5. Plots of activity normalized to mass and different measures of surface acidity are located in S15 and S17.

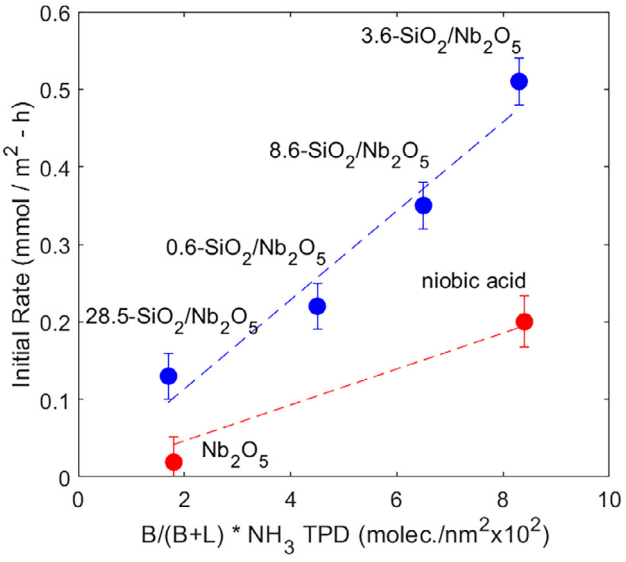

Fig. 7. Proportionality between tetrahydropyranylation rates (as in Fig. 6) and a proxy for the Brønsted acid site density from pyridine DRIFTS. The latter is defined as the fractional area of the Bronsted acid feature at 1540 cm^{-1} relative to the sum of the Brønsted and Lewis features (1445 cm^{-1}). That fraction is multiplied by the total acidity as determined by NH_3 TPD (Table 2). See Table S11 for values.

and strong sites determined from NH_3 TPD are also ineffective in normalizing tetrahydropyranylation rates across the range of SiO_2 loadings. As shown in Fig. 7, tetrahydropyranylation rates do appear to be proportional to the Brønsted sites determined from pyridine DRIFTS. Absent the ability to quantify absolute numbers of sites directly from pyridine DRIFTS, the number of these acid sites is assumed to be proportional to the total acid sites from NH_3 TPD multiplied by the relative fraction of Brønsted sites seen in the pyridine DRIFTS spectra. Critically, two trend-lines emerge, where the specific activity (the slope of the trendline) of the SiO_2/Nb_2O_5 materials is higher than that of niobic acid or calcined Nb_2O_5, consistent with the lower apparent activation barrier for the SiO_2/Nb_2O_5 materials. The structure of the putative SiO_2/Nb_2O_5 Brønsted site (Scheme 1) appears to be more proficient at adsorbing and activating dihydropyran than is an acid site on bare Nb_2O_5.

4. Conclusions

In this study, a series of overcoated SiO_2 on Nb_2O_5 materials were synthesized to create and probe acidity at the silica-niobia interface. The deposition of SiO_2 impacts the total number and the distribution of acid sites, which are increased relative to calcined Nb_2O_5 at low SiO_2 loadings and decrease as the surface becomes siliceous. The deposition of SiO_2 also generates new features in the pyridine DRIFTS spectra, notably silanol groups at 3745 cm^{-1} whose depletion is correlated with the formation of protonated pyridine at 1540 cm^{-1}. These features are both most prominent at sub-monolayer SiO_2 loadings, suggesting that the Brønsted sites formed at the silica-niobia interface are pseudo-bridging silanols formed between surface Si-OH and residual undercoordinated, Lewis acidic Nb atoms on the uncovered the oxide surface.

The activity of SiO_2/Nb_2O_5 in the hydroalkoxylation of 2,4-dihydropyran with n-octanol is also maximized at intermediate SiO_2 loadings, with a maximum activity of 0.51 mmol / m^2 – h at 3.6 Si / nm^2, or a Si / surface Nb ratio of ~0.5, that is significantly higher than the activities we measured over niobic acid (0.20 mmol / m^2 – h) and calcined Nb_2O_5 (0.02 mmol / m^2 – h). Similar reaction

rates over the series of SiO_2/Nb_2O_5 –c controls provide strong evidence that this enhanced activity is due to newly formed Brønsted sites at the silica-niobia interface. Decreasing activity observed at higher SiO_2 loadings is likely due to the silica-niobia interface becoming inaccessible. The hydroalkoxylation rates scale in proportion to the Brønsted acidity revealed by pyridine DRIFTS, and they remain higher for SiO_2/Nb_2O_5 than for niobic acid or Nb_2O_5 even on this basis. Lastly, slightly lower apparent hydroalkoxylation activation energies over SiO_2/Nb_2O_5 provide further evidence that the sites located at the silica-niobia interface are more active than those found on niobic acid.

In this work we have extended our use of overcoated materials, previously used to study SiO_2/Al_2O_3 and SiO_2/TiO_2, to demonstrate the platform's utility in studying the chemistry of SiO_2/Nb_2O_5 materials. In this application, the highly tunable overcoating process has provided additional understanding of the active sites that form at the SiO_2 – Nb_2O_5 interface, showing that the SiO_2 loading can be controlled to influence the properties of the composite material. Future work is aimed toward applying this synthesis approach to study the acidity of additional SiO_2-MO_x interfaces, expand the reaction scope to higher temperature gas phase reactions, and to probe the structure of surface species with solid state NMR.

Funding sources

This material is based upon work supported by the U.S. Department of Energy, Office of Science, Office of Basic Energy Sciences under Award Number DOE DE-FG02-03-ER154757 for support of M.A.A., S.A. and the National Science Foundation under Cooperative Agreement No. EEC-1647722 for support of A.T.Y.W.

Declaration of Competing Interest

The authors declare that they have no known competing financial interests or personal relationships that could have appeared to influence the work reported in this paper.

Acknowledgment

A.T.Y.W. would like to thank Vincent Cheng for assistance with running tetrahydropyranylation reactions. A.T.Y.W thanks Mihir Bhagat for assistance with method development for GC-MS analyses.

This material is based upon work supported by the U.S. Department of Energy, Office of Science, Office of Basic Energy Sciences under Award Number DOE DE-FG02-03ER15457 for support of M.A.A. and S.A. and the National Science Foundation under Cooperative Agreement No. EEC-1647722 for support of A.T.Y.W.

Metal analysis was performed at the Northwestern University Quantitative Bio-element Imaging Center. This work made use of the EPIC facility of Northwestern University's NU*ANCE* Center, which has received support from the Soft and Hybrid Nanotechnology Experimental (SHyNE) Resource (NSF ECCS-1542205); the MRSEC program (NSF DMR-1720139) at the Materials Research Center; the International Institute for Nanotechnology (IIN); the Keck Foundation; and the State of Illinois, through the IIN. This work made use of the Jerome B.Cohen X-Ray Diffraction Facility supported by the MRSEC program of the National Science Foundation (DMR-1720139) at the Materials Research Center of Northwestern University and the Soft and Hybrid Nanotechnology Experimental (SHYNE) Resource (NSF ECCS-1542205.) The REACT Core facility acknowledges funding from the Department of Energy (DE-FG02-03ER15457) used for the purchase of the Altamira AMI-200 and the Nicolet 6700 FT-IR.

Appendix A. Supplementary material

Additional SiO_2/Nb_2O_5 sample information, N_2 physisorption isotherms, NLDFT micropore distributions, comparison XRD patterns after secondary calcination, raw first cycle propylamine TPRx data, Hammett Indicator experiments, cyclic propylamine TPRxn values, full pyridine DRIFTS spectra, full NH_3 DRIFTS spectra, pyridine desorption DRIFTS spectra, preliminary tetrahydropyranylation over SiO_2/Al_2O_3 catalyst, summary of catalytic data, mass-normalized Tetrahydropyranylation rates, Arrhenius plots for SiO_2/Nb_2O_5 and niobic acid, NH_3 and propylamine TOF plots. Supplementary data to this article can be found online at https://doi.org/10.1016/j.jcat.2020.10.027.

References

[1] K. Tanabe, Application of niobium oxides as catalysts, Catal. Today. 8 (1990) 1–11.
[2] T. Iizuka, K. Ogasawara, K. Tanabe, Acidic and catalytic properties of niobium pentaoxide, Bull. Chem. Soc. Jpn. 56 (1983) 2927–2931.
[3] K. Nakajima, J. Hirata, M. Kim, N.K. Gupta, T. Murayama, A. Yoshida, N. Hiyoshi, A. Fukuoka, W. Ueda, Facile formation of lactic acid from a triose sugar in water over niobium oxide with a deformed orthorhombic phase, ACS Catal. 8 (2018) 283–290, https://doi.org/10.1021/acscatal.7b03003.
[4] K. Nakajima, Y. Baba, R. Noma, M. Kitano, J.K. Kondo, S. Hayashi, M. Hara, Nb2O5*3nH2O as a heterogeneous catalyst with water-tolerant lewis acid sites, J. Am. Chem. Soc. 133 (2011) 4224–4227, https://doi.org/10.1021/ja110482r.
[5] G.S. Foo, D. Wei, D.S. Sholl, C. Sievers, Role of Lewis and Brønsted acid sites in the dehydration of glycerol over niobia, ACS Catal. 4 (2014) 3180–3192, https://doi.org/10.1021/cs5006376.
[6] P. Lauriol-Garbey, G. Postole, S. Loridant, A. Auroux, V. Belliere-Baca, P. Rey, J. M. Millet, Acid – base properties of niobium-zirconium mixed oxide catalysts for glycerol dehydration by calorimetric and catalytic investigation, Appl. Catal. B Environ. 106 (2011) 94–102, https://doi.org/10.1016/j.apcatb.2011.05.011.
[7] C. Tagusagawa, A. Takagaki, A. Iguchi, K. Takanabe, J.N. Kondo, K. Ebitani, S. Hayashi, T. Tatsumi, K. Domen, Highly active mesoporous Nb – W oxide solid-acid catalyst, Angew. Chem. Int. Ed. 49 (2010) 1128–1132, https://doi.org/10.1002/anie.200904791.
[8] M. Ziolek, Niobium-containing catalysts — the state of the art, Catal. Today. 78 (2003) 47–64.
[9] M.S.P. Francisco, R. Landers, Y. Gushikem, Local order structure and surface acidity properties of a Nb2O5 / SiO2 mixed oxide prepared by the sol – gel processing method, J. Solid State Chem. 177 (2004) 2432–2439, https://doi.org/10.1016/j.jssc.2004.03.035.
[10] C.G. Lugmair, T.D. Tilley, Single source molecular precursors to niobia – silica and niobium phosphate materials, Monatshefte Fur Chemie. 137 (2006) 557–566, https://doi.org/10.1007/s00706-006-0445-9.
[11] A. Aronne, E. Marenna, V. Califano, E. Fanelli, P. Pernice, M. Trifuoggi, A. Vergara, Sol – gel synthesis and structural characterization of niobium-silicon mixed-oxide nanocomposites, J. Sol-Gel Sci. Technol. 43 (2007) 193–204, https://doi.org/10.1007/s10971-007-1563-5.
[12] P. Carniti, A. Gervasini, M. Marzo, Silica – niobia oxides as viable acid catalysts in water: effective vs. intrinsic acidity, Catal. Today. 152 (2010) 42–47, https://doi.org/10.1016/j.cattod.2009.07.111.
[13] J. Datka, A.M. Turek, J.M. Jehng, I.E. Wachs, Acidic properties of supported niobium oxide catalysts: an infrared spectroscopy investigation, J. Catal. 135 (1992) 186–199, https://doi.org/10.1016/0021-9517(92)90279-Q.
[14] P.A. Burke, E. Ko, Acidic properties of oxides containing niobia on silica and niobia in silica, J. Catal. 46 (1991) 38–46.
[15] M. Niwa, N. Katada, Y. Murakami, Generation of acid sites by SiO2 deposition on groups IVB metal oxides, J. Catal. 134 (1992) 340–348.
[16] M.A. Ardagh, Z. Bo, S.L. Nauert, J.M. Notestein, Depositing SiO2 on Al2O3: a route to tunable bronsted acid catalysts, ACS Catal. 6 (2016) 6156–6164, https://doi.org/10.1021/acscatal.6b01077.
[17] A.R. Mouat, C. George, T. Kobayashi, M. Pruski, R.P. Van Duyne, T.J. Marks, P.C. Stair, Highly dispersed SiO x / Al 2 O 3 catalysts illuminate the reactivity of isolated silanol sites, Angew. Commun. 54 (2015) 13346–13351, https://doi.org/10.1002/anie.201505452.
[18] A.R. Mouat, T. Kobayashi, M. Pruski, T.J. Marks, P.C. Stair, Direct spectroscopic evidence for isolated silanols in SiO $_x$ /Al $_{2\ O}$ 3 and their formation mechanism, J. Phys. Chem. C. 121 (2017) 6060–6064, https://doi.org/10.1021/acs.jpcc.6b11196.
[19] Z. Bo, T.R. Eaton, J.R. Gallagher, C.P. Canlas, J.T. Miller, J.M. Notestein, Size-selective synthesis and stabilization of small silver nanoparticles on TiO2 partially masked by SiO2, Chem. Mater. 27 (2015) 1269–1277, https://doi.org/10.1021/cm504243f.
[20] Z. Yang, Y. Li, Q. Wu, N. Ren, Y. Zhang, Z. Liu, Y. Tang, Layered niobic acid with self-exfoliatable nanosheets and adjustable acidity for catalytic hydration of

ethylene oxide, J. Catal. 280 (2011) 247–254, https://doi.org/10.1016/j.jcat.2011.03.026.
[21] J. Rouquerol, P. Llewellyn, F. Rouquerol, Is the BET equation applicable to microporous adsorbents ?, in: Stud. Surf. Sci. Catal., Elsevier B.V., 2007: pp. 49–56. https://doi.org/10.1016/S0167-2991(07)80008-5.
[22] G. Kupgan, T.P. Liyana-arachchi, C.M. Colina, NLDFT pore size distribution in amorphous microporous materials, Langmuir. 33 (2017) 11138–11145, https://doi.org/10.1021/acs.langmuir.7b01961.
[23] S.H. Madani, L.H. Diaz, M.J. Biggs, P. Pendleton, Uncertainty in pore size distribution derived from adsorption isotherms: II. Adsorption integral approach, Microporous Mesoporous Mater. 214 (2015) 217–223, https://doi.org/10.1016/j.micromeso.2015.04.030.
[24] O. Kresnawahjuesa, R.J. Gorte, D. De Oliveira, L.Y. Lau, A simple, inexpensive, and reliable method for measuring Bronsted- acid site densities in solid acids, Catal. Lett. 82 (2002) 155–160.
[25] V. Lebarbier, M. Houalla, T. Onfroy, New insights into the development of Brønsted acidity of niobic acid, Catal. Today. 192 (2012) 123–129, https://doi.org/10.1016/j.cattod.2012.02.061.
[26] D. Pradhan, A.W. Wren, S.T. Misture, N.P. Mellott, Investigating the structure and biocompatibility of niobium and titanium oxides as coatings for orthopedic metallic implants, Mater. Sci. Eng. C. 58 (2016) 918–926, https://doi.org/10.1016/j.msec.2015.09.059.
[27] O. Yamaguchi, T. Kanazawa, K. Shimizu, Crystallization of amorphous silica into quartz, J. Chem. Soc. Dalt. Trans. (1982) 1005–1007, https://doi.org/10.1017/CBO9781107415324.004.
[28] K. Kraffert, M. Karg, R. Schmack, G. Clavel, C. Boissiere, T. Wirth, N. Pinna, R. Kraehnert, Stabilization of mesoporous iron oxide films against sintering and phase transformations via atomic layer deposition of alumina and silica, Adv. Mater. Interfaces. 5 (2018) 1800360, https://doi.org/10.1002/admi.201800360.
[29] J.N. Kondo, K. Domen, Crystallization of mesoporous metal oxides, Chem. Mater. 20 (2008) 835–847.
[30] J.M.R. Gallo, D. Wang, H.N. Pham, J.A. Libera, C.L. Marshall, W. Elam, A.K. Datye, J.A. Dumesic, Synthesis of highly ordered hydrothermally stable mesoporous niobia catalysts by atomic layer deposition, ACS Catal. 1 (2011) 1234–1245, https://doi.org/10.1021/cs200367t.
[31] J.G. Weissman, E.I. Ko, P. Wynblatt, Study of the morphology and structure of niobia-silica surface oxides using model thin films, J. Catal. 108 (1987) 383–400, https://doi.org/10.1016/0021-9517(87)90187-4.
[32] K. Tanabe, Niobic acid as an unusual acidic solid material, Mater. Chem. Phys. 7 (1987) 217–225.
[33] J. He, Q.J. Li, Y.N. Fan, Dispersion states and acid properties of SiO2-supported Nb 2O5, J. Solid State Chem. 202 (2013) 121–127, https://doi.org/10.1016/j.jssc.2013.03.040.
[34] S.-H. Chai, H.-P. Wang, Y. Liang, B.-Q. Xu, Sustainable production of acrolein: gas-phase dehydration of glycerol over Nb2O5 catalyst, J. Catal. 250 (2007) 342–349, https://doi.org/10.1016/j.jcat.2007.06.016.
[35] S.A. Bates, W.N. Delgass, F.H. Ribeiro, J.T. Miller, R. Gounder, Methods for NH3titration of Brønsted acid sites in Cu-zeolites that catalyze the selective catalytic reduction of NOx with NH3, J. Catal. 312 (2014) 26–36, https://doi.org/10.1016/j.jcat.2013.12.020.
[36] M. Hiyoshi, B. Lee, D. Lu, M. Hara, J.N. Kondo, K. Domen, Supermicroporous niobium oxide as an acid catalyst, Catal. Letters. 98 (2004) 1–6.
[37] H.N. Pham, Y.J. Pagan-torres, J.C. Serrano-ruiz, D. Wang, J.A. Dumesic, A.K. Datye, Improved hydrothermal stability of niobia-supported Pd catalysts, Appl. Catal. A Gen. 397 (2011) 153–162, https://doi.org/10.1016/j.apcata.2011.02.026.
[38] C.P. Kumar, K.R. Reddy, V.V. Rao, Vapour phase ammoxidation of toluene over vanadium oxide supported on Nb2O5-TiO2, Green Chem. 4 (2002) 513–516, https://doi.org/10.1039/b206581a.
[39] M. Anilkumar, W.F. Hoelderich, New non-zeolitic Nb-based catalysts for the gas-phase Beckmann rearrangement of cyclohexanone oxime to caprolactam, J. Catal. 293 (2012) 76–84, https://doi.org/10.1016/j.jcat.2012.06.007.
[40] Z. Zhang, P. Wang, Z. Wu, C. Yue, X. Wei, J. Zheng, M. Xiang, B. Liu, Efficient synthesis of niobium pentoxide nanowires and application in ethanolysis of furfuryl alcohol †, RSC Adv. 10 (2020) 5690–5696, https://doi.org/10.1039/d0ra00085j.
[41] Y. Duan, J. Zhang, D. Li, D. Deng, L. Ma, Y. Yang, Direct conversion of carbohydrates to diol by the combination of niobic acid and a hydrophobic ruthenium catalyst †, RSC Adv. 7 (2017) 26487–26493, https://doi.org/10.1039/c7ra03939e.
[42] J.G. Tittensor, R.J. Gorte, D.M. Chapman, Isopropylamine adsorption for the characterization of acid sites in silica-alumina catalysts, J. Catal. 720 (1992) 714–720.
[43] W.E. Farneth, R.J. Gorte, Methods for characterizing zeolite acidity, Chem. Rev. 95 (1995) 615–635, https://doi.org/10.1021/cr00035a007.
[44] D.J. Parrillo, A.T. Adamo, G.T. Kokotailo, R.J. Gorte, Amine adsorption in H-ZSM-5, Appl. Catal. 67 (1990) 107–118.
[45] K. Zhang, D.M. Zimmerman, A. Chung-phillips, C.J. Cassady, Experimental and ab initio studies of the gas-phase basicities of polyglycines, J. Am. Chem. Soc. 115 (1993) 10812–10822, https://doi.org/10.1021/ja00076a044.
[46] J. Briggs, R. Yamdagni, P. Kebarle, Intrinsic basicities of ammonia, methylamines, anilines, and pyridine from gas-phase proton exchange equilibria, J. Am. Chem. Soc. 94 (1972) 5128–5130, https://doi.org/10.1021/ja00769a081.
[47] H. Shima, M. Tanaka, H. Imai, T. Yokoi, T. Tatsumi, J.N. Kondo, IR observation of selective oxidation of cyclohexene with H2O2 over mesoporous Nb2O5, J. Phys. Chem. C. 113 (2009) 21693–21699.
[48] L.T. Zhuravlev, The surface chemistry of amorphous silica. Zhuravlev model, Colloids Surf. Physicochem. Eng. Asp. 173 (2000) 1–38, https://doi.org/10.1016/S0927-7757(00)00556-2.
[49] Z. Xue, Y. Zhang, G. Li, J. Wang, W. Zhao, T. Mu, Niobium phytate prepared from phytic acid and NbCl5: a highly efficient and heterogeneous acid catalyst, Catal. Sci. Technol. 6 (2016) 1070–1076, https://doi.org/10.1039/c5cy01123j.
[50] C. Chizallet, P. Raybaud, Pseudo-bridging silanols as versatile brønsted acid sites of amorphous aluminosilicate surfaces, Angew. Chemie - Int. Ed. 48 (2009) 2891–2893, https://doi.org/10.1002/anie.200804580.
[51] F. Leydier, C. Chizallet, A. Chaumonnot, M. Digne, E. Soyer, A.A. Quoineaud, D. Costa, P. Raybaud, Brønsted acidity of amorphous silica-alumina: the molecular rules of proton transfer, J. Catal. 284 (2011) 215–229, https://doi.org/10.1016/j.jcat.2011.08.015.
[52] B. Chakraborty, B. Viswanathan, Surface acidity of MCM-41 by in situ IR studies of pyridine adsorption, Catal. Today. 49 (1999) 253–260.
[53] M. Valla, A.J. Rossini, M. Caillot, P. Raybaud, M. Digne, A. Chaumonnot, A. Lesage, L. Emsley, J.A. Van Bokhoven, Atomic Description of the Interface between Silica and Alumina in Aluminosilicates through Dynamic Nuclear Polarization Surface- Enhanced NMR Spectroscopy and First-Principles Calculations, (2015). https://doi.org/10.1021/jacs.5b06134.
[54] F.A. Perras, Z. Wang, T. Kobayashi, A. Baiker, J. Huang, M. Pruski, Shedding light on the atomic-scale structure of amorphous silica – alumina and its Brønsted acid sites, PCCP. 21 (2019) 30–33, https://doi.org/10.1039/c9cp04099d.
[55] I. Rodriguez, M.J. Climent, S. Iborra, V. Fornes, A. Corma, Use of delaminated zeolites (ITQ-2) and Mesoporous molecular sieves in the production of fine chemicals: preparation of dimethylacetals and tetrahydropyranylation of alcohols and phenols, J. Catal. 192 (2000) 441–447.
[56] N. Miyashita, A. Yoshikoshi, P.A. Grieco, Pyridinium p-toluenesulfonate. A mild and efficient catalyst for the tetrahydropyranylation of alcohols, J. Org. Chem. 42 (1977) 3772–3774, https://doi.org/10.1021/jo00443a038.
[57] M. Shibuya, S. Fujita, M. Abe, Y. Yamamoto, Brønsted acid/silane catalytic system for intramolecular hydroalkoxylation and hydroamination of unactivated alkynes, ACS Catal. 7 (2017) 2848–2852, https://doi.org/10.1021/acscatal.7b00403.
[58] N. Tsuji, J.L. Kennemur, T. Buyck, S. Lee, S. Prévost, P.S.J. Kaib, D. Bykov, C. Farès, B. List, Activation of olefins via asymmetric Brønsted acid catalysis, Science (80-) 359 (2018) 1501–1505.
[59] G. Sartori, R. Ballini, F. Bigi, G. Bosica, R. Maggi, P. Righi, Protection (and deprotection) of functional groups in organic synthesis by heterogeneous catalysis, Chem. Rev. 104 (2004) 199–250, https://doi.org/10.1021/cr0200769.
[60] H. Qian, X. Han, R.A. Widenhoefer, Platinum-catalyzed intramolecular hydroalkoxylation of γ - and δ -hydroxy olefins to form cyclic ethers, JACS Commun. 126 (2004) 9536–9537, https://doi.org/10.1021/ja0477773.
[61] X. Yu, S. Seo, T.J. Marks, Effective, selective hydroalkoxylation / cyclization of alkynyl and allenyl alcohols mediated by lanthanide catalysts, JACS Commun. 129 (2007) 7244–7245, https://doi.org/10.1021/ja071707p.
[62] Y. Oe, T. Ohta, Y. Ito, Ruthenium-catalyzed addition reaction of alcohols across olefins, Synlett. 1 (2005) 179–181, https://doi.org/10.1055/s-2004-836058.
[63] E. Marotta, E. Foresti, T. Marcelli, F. Peri, P. Righi, N. Scardovi, G. Rosini, CeCl3, 7H2O – NaI catalyzed hydrooxacyclization of unsaturated 3-hydroxy esters, Org. Lett. 4 (2002) 4451–4453, https://doi.org/10.1021/ol026955z.
[64] T. De Baerdemaeker, W. Vandebroeck, H. Gies, B. Yilmaz, U. Müller, M. Feyen, D. De Vos, Shape-selective organic – inorganic zeolitic catalysts prepared via interlayer expansion, Catal. Today. 235 (2014) 169–175, https://doi.org/10.1016/j.cattod.2014.02.035.
[65] G.P. Romanelli, J.C. Autino, M.N. Blanco, L.R. Pizzio, Tungstosilicate salts as catalysts in phenol tetrahydropyranylation and depyranylation, Appl. Catal. A Gen. 295 (2005) 209–215, https://doi.org/10.1016/j.apcata.2005.08.019.
[66] M.V. Shamzhy, C. Ochoa-Hernández, V.I. Kasneryk, M.V. Opanasenko, M. Mazur, Direct incorporation of B, Al, and Ga into medium-pore ITH zeolite: synthesis, acidic, and catalytic properties, Catal. Today. 277 (2016) 37–47, https://doi.org/10.1016/j.cattod.2015.10.013.
[67] N. Azizi, M. Abdoli-Senejani, F. Abbasi, An efficient Brønsted-Lewis acidic ionic liquid catalyzed tetrahydropyranylation of alcohols, Tetrahedron Lett. 57 (2016) 5009–5011, https://doi.org/10.1016/j.tetlet.2016.09.099.